ERRORS DERIVED FROM UNCERTAINTY IN THE ACCURACY OF THE CANADIAN NATIONAL TOPOGRAPHIC SERIES 1:50000 MAPS

by
M. Lasserre

Canada Centre for Remote Sensing

RÉSUMÉ

On a constaté des variations dans les élévations enregistrées pour le même site géographique sur les cartes NTS compilées à 18 ans d'intervalle. L 'historique des compilations cartographiques a été passé en revue. I1 est ressorti de cette étude que les changements dans les techniques de cartographie - contrôle accru sur le plan géodésique et photogrammétrique - et les differences dans l'utilisation du sol constituent des facteurs importants de changement dans les élévations réprésentées dérivées d'élévation pour les anciennes et les nouvelles cartes de sites identiques ont été calculées. Des mesures d'incertitude en ont été déduites, en utilisant les angles d'illumination incidente et les angles solaires effectifs, et ont servi à évaluer les erreurs associées au fait de ne pas connaître la précision des cartes et de ne pas en tenir compte dans les calculs nécessitant des modèles numériques d'élévation.

SUMMARY

Elevations recorded for the same geographic location on NTS maps compiled 18 years apart were found to vary. The map compilation history was studied, and changes in mapping technology, expanded geodetic and photogrammetric control, and land use practices were found to be important components of the mapped-elevation changes. The elevation derivatives for old and new compilations of identical areas were calculated, and illumination incidence angle, as well as effective sun angle, uncertainties were used to examine the effects of not knowing the map accuracy and not applying it in calculations requiring digital elevation models.

INTRODUCTION

The requirements for a digital elevation model (DEM) were realized in a project under way at the Canada Centre for Remote Sensing (CCRS) (Fung and Lasserre, 1987; Goodenough *et al.,* 1988). Two adjacent elevation basis from the National Topographic Series (NTS) maps at a scale of 1:50000 were acquired from the Surveys and Mapping Branch (now Surveys, Mapping and Remote Sensing Sector, The Canada Centre for Mapping) of the Department of Energy, Mines and Resources. There was found to be a discontinuity in the elevation match at the join of these two maps (Figure 1), and both elevation discrepancy and slope-aspect changes could not be rationalized by normal intuition. The history of the map compilations was acquired (MacDonald, 1986), and a synopsis of the different aspects of map production is contained in Table 1. A detailed description of the stereo plotter and adjustment components in Table 1 can be found in Slama (1980).

It was clear that most major components of map production had significantly changed over the interim 18-year period separating the compilation of the two map sheets (82G13, 82G14) and that only a recompilation of the older map (82G14) could resolve the discontinuities. The Surveys and Mapping Branch (Gagné, 1986) recompiled elevations and hydrography for the test area (approximately 6 km x 12 km), which was being studied in the project and which lay in the northwest corner of the older map sheet. This recompilation used the adjacent photogrammetric control for 82G13, which fortuitously spanned the entire test area.

When the compilation was completed, it was judged to have the same accuracy standard, planimetric, and elevation as 82G13. In achieving this seamless elevation coverage, the requirements of the aforementioned project were met; but the study for this present paper continued by defining a premise that assumed the remote sensing user of NTS maps may be *unknowing* of the map's accuracy. Also, the user may be unaware of what magnitude of error could be anticipated by using the elevation data derived from the map contours through manipulation of DEMs into slope, slope-aspect, and illumination incidence angle. Generalization of the results given in this paper to other terrain or other map accuracy discrepancies was not intended, but the magnitude of the uncertainties should alert users to potential errors in elevations interpolated from some topographic maps.

From the new compilation and the old NTS map basis, digital vectors were created from the contours. Although this occurred by automated means, the object was to replicate the use of NTS maps by those wanting elevation information in a digital form. Both old and new elevation contours were gridded into a digital elevation model as a raster representation without the use of break lines (hydrography excepted) or control other than what was definable on the map.

Uncontrolled DEM griding has been studied by Clarke *et al.* (1982). For the present study, with the following of identical process paths from vector contours to gridded elevation models for both compilations, it was assumed that random but statistically identical errors were contributed to both data sets. The data were

Table 1
Map compilation history for 82G13 and 82G14. The new elevations compiled for 82G14 would have the same specifications listed here for 82G13

Map Sheet ->	82G13	82G14
Accuracy Classification*	A2-100'**	C3-100″
Photo Dates	1970,71	1954
Date of Current Basis	1970	1955
Last Revision	1979	1979
Published	1980	1980
Stereo Plotter	second order	less than second order
Adjustment	PAT M (numerical)	slotted template

* (CCM 1989; NATO 1983). The literal 'A' implies planimetric accuracy of ½ mm at map scale (for 90 per cent of all points of detail), and in "C" it is 2 mm. The numeric is for elevation accuracy, and a '2' means that 90 per cent of all contours are within 1 contour interval (in this case, the interval is 100 ft, which is shown as the third quantity). For Canadian maps, '3' implies that the data is between 1 and 2 contour intervals, and for the calculations in this paper the value of 1.5 was used.

** 82G13 was compiled and adjusted within a large adjustment block (H001) using new geodetic and altimetric data. The block was numerically adjusted giving an overall rating of A2 to A3 for 10 m contours. The A2 classification given here for 82G13 is for the published manuscripted map.

gridded at 25 m and 100 m, the grids were used to generate a cubic polynomial in each 3 x 3 neighbourhood, and slopes and slope-aspects were calculated at the same grid intervals. The slope is the gradient as calculated from the polynomial, and the slope/aspect is the direction of the gradient, with North at zero degrees and East at 90 degrees. Further analysis of these data sets, including incidence and sun angles, involved the creation of statistical moments for the differences between each of the like variables. For instance, the two compiled elevations were differenced, and the distribution of the differences was calculated. These statistics are summarized in Table 2. Through the A2 accuracy, achieved for the new compilation of the test area in 82G14, it was assumed that a total description of the topographic content of an image pixel's energy would be possible.

The grid intervals that were chosen were based on two commonly used pixel areas for remote sensing image data and were assumed to be within minimum sampling criterion for the test area's terrain. Each grid was formed through the same process and used the same vectored contours as support for interpolation. Each grid value was a point value calculated for the same relative geographic location within the cell, and the loo m grid does not represent an averaging process based on 25 m elements.

The rationale for describing terrain relief uncertainty in terms of the sun angles (azimuth and elevation) can be explained by referring to the analysis in Appendix I. Briefly, two co-ordinate spaces are assigned: one to the DEM that was acquired and that, with reference to the real world, may be classified to have an accuracy of C3; the second to the topographic description that has the highest possible accuracy and that is assumed to be coincident with remotely sensed data (such as from Landsat). The propagation of errors from Ground Control Point (GCP) identification is not addressed here, and the image may have been geocoded with GCPs taken from maps of unknown or possibly varying accuracy standards. Both of these reference spaces are relative to an invariant Cartesian reference space, which contains the geographic position of the grid cells and from which the sun angles are calculated. With reference to Figure AI.l, when moving from the unprimed space to the primed space (i.e., moving from terrain described with an accuracy of C3 to one of accuracy A2), there would be no translation as the origin of both of these spaces does not move in the cartesian co-ordinate system (XI, X2, X3). This rotation of one space to the other if fixed to the sun (**S** in Figure AI.2) would cause the sun's position to artificially change to **S'**, and the sun angles, which are normally calculated from an invariant geocentric co-ordinate system, will vary with the transformation. Therefore, the trajectories of the sun in space can be used to describe the uncertainty in a system where both map and image co-ordinate systems are assumed to coincide. This assumption of coincidence is analogous to the premise stated earlier, that is, of not knowing the uncertainty of relief components taken from a map.

It was felt that the calculation of the incident angle variation does not satisfactorily describe the directional contribution from non-isotropic topography in the same way as both sun azimuth and elevation would do. For instance, if the topography were purely random in relief slope and slope-aspect, a radially symmetrical uncertainty in illumination incidence angle would be useful. In the present case, it was clear that terrain features, such as ridges and rivers, contributed to the linear trends. For example, the departure from symmetry in the statistics for slope-aspect, with a mean of 186° and a mode of 251° (Table 2), infers some linear features in the SE direction. Frequency distributions with skewness ranges from + 3. to -3. implies, also, that simple mean and standard deviation interpretation of the sun angles might be misleading. In the present descriptive context, however, these asymmetries were ignored.

With reference to Figure 2, by investigating areas with known large disparities in the A-A' rotation (θ in Figure AI.2), it was found that a shift in planimetry of breakpoints in topography can severely influence the differences in slope-aspect by contributing large positive or negative values. Using differences with magnitudes of less than 90° and then recomputing the statistics for illumination incidence angle variations, as well as sun angle differences, the 100 m grid data did not change its RMS error by more than 0.1°. However, for the 25 m data, a 2.1° (18 per cent) reduction in sun azimuth RMS error was obtained and both sun elevation and illumination incidence angle RMS errors decreased by less than 10 per cent.

It would be necessary to conduct further research into the spatial origins of the DEM discrepancies, but without heuristics or data-dependent rules concerning these origins, the results would

Table 2
Statistical summary for differences derived from old and new elevations for the test area part of 82G14. Edge effects from interpolations that reach end-of-data have been eliminated, and the total number of points used in the calculation was 6875 for a 100 m grid and 109200 for a 25 m grid. Statistics for elevation, slope, and aspect were calculated from the new compilation

	MIN	MAX	MEAN	σ	MODE	SKEWNESS	KURTOSIS
100 Metres							
Elevation (M)	1499	2314	1857	174	1887	.2	−.5
△Elevation	−73	112	11	26	5	.1	.3
Slope (deg)	0	46	17	7	17	.3	−.2
△Slope	16	−40	0	4	0	−1	13
Aspect (deg)	0	359	186	108	251	−.1	−1
△Aspect	177	−178	−1	21	−1	−1	22
θ (deg)*, **	0	44	4	3	2	3	20
△Incidence-angle (deg)*	−37	13	.3	3	−.1	−3	25
△Emergent-angle (deg)***	−0	42	3	3	.8	3	21
△Sun elevation (deg)*	−13	35	.1	3	−1	2	14
△Sun azimuth (deg)*	−36	24	−.8	5	−1	−.3	3
25 Metres							
Elevation (M)	1498	2333	1873	173	1819	.3	−.5
△Elevation	−77	125	10	28	13	.1	.3
Slope (deg)	0	61	20	9	14	.2	−.3
△Slope	38	−43	1	7	0	0	2
Aspect (deg)	0	360	187	107	243	−.1	−1
△Aspect	−180	180	−1	34	1	.4	8
θ (deg)*, **	0	71	8	7	4	2	8
△Incidence-angle (deg)*	−38	36	.4	6	−1	0	2
△Emergent-angle (deg)***	0	68	7	6	3	2	9
△Sun elevation (deg)*	−32	51	.2	6	−.1	.6	3
△Sun azimuth (deg)*	−110	140	−.9	12	−.9	.1	8

* The quantities refer to variables defined in Figure AI.2

** Defined as the angle between surface normals for identical DEM grid cells in both old and new map compilations

*** Calculated by setting the illumination vector (a_1, a_2, a_3) to (0,0,1)

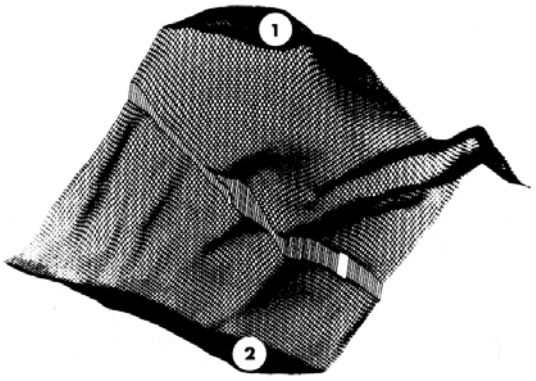

Figure 1
Wire mesh description for the join between the 1:50000 scale NTS maps 82G13 (2) and 82G14 (1). The 'rift' was caused by changes in surface cover type during successive air photo capture and technology changes affecting stereo plotting and adjustment spanning an 18-year period.

probably lack both in generality and in independence of terrain type and map compilation histories. Investigations of terrain measurement error statistics (Ostman, 1987) indicate that errors in interpolated elevations are non-stationary stochastic processes. The lack of normality in elevation distributions and systematic fluctuations in the relief makes the estimation of correlation terms difficult and dependent on spatially varying terrain features (Fredericksen *et al.,* 1984).

SOURCES OF ERROR

From the database at the Topographic Survey Division (Surveys and Mapping Branch), which contains the history of compilation and revision for the NTS 1:50000 map series, the most important differences in the making of maps 82G13 and 82G14 could be determined. There seemed to be sufficient change derived from the technological advances in adjustment methods, stereo plotting, and the amount and accuracy of survey control over the period of 18 years between the map sheet compilations that planimetric variations, such as the location of river courses and the difference in absolute elevations, could be explained. The changes in landscape features, for example, that deduced from the generally smooth contours in 82G14 versus the crenelated contours of 82G13, could be explained in some cases by the logging practices in the test area (BCMF, 1987), which occurred between the maps' respective photographic coverage. Cartographic generalization applied to maps with a low accuracy would lead to elevation smoothing and could be expected where dense forests prevent

elevation measurement on the ground. The continuation of a noticeable relief feature in 82Gl3 (Figure 1) was missing in 82G14 but was restored by the new compilation of 82G14. It was concluded that this anomaly was a product of the change in cover density, as well as elevation compilation technology change.

The accuracy of a published map (σ_m) can be determined by (CCSM, 1984):

$$\sigma_m = (\sigma^2 \text{ control} + \sigma^2 \text{ photography} + \sigma^2 \text{ triangulation} + \sigma^2 \text{ orientation} + \sigma^2 \text{ compilation} + \sigma^2 \text{ drafting} + \sigma^2 \text{ printing} + \sigma^2 \text{ digitization})^{1/2}.$$

The term for digitization was included for a digital representation of source material, which originated as manuscripted maps. The precision of contour data has been discussed in detail by Richardus (1973), and the error in formation of DEMs through the process of digital griding from contours is given in Clarke *et al.* (1982). The vector data derived from scanning a map contour basis were within a line width at the map scale, and the griding interval was calculated to be within the limits defined by Peucker *et al.* (1976).

Peucker calculated the minimum grid sample interval on the basis of total map error by equating the grid error, plus the planimetric point error at the contour points, to the total map error. The effect of Peucker's assumptions, that is, uniform slopes and zero covariance between planimetric and vertical errors in control and contour positions, as well as the neglecting of random errors in map drafting and printing, can be estimated by using these terms in the complete map accuracy description given in Richardus (1973). The addition of the covariance term contributes, in one heuristic estimate of its magnitude, to about 12 per cent to the total map error estimated by Peucker. In the present work, only those terms used by Peucker are considered since they would be the ones most available to users of topographic maps.

A linear relationship between grid size and the interpolation error was adopted, and with the approximation given in Clarke *et al.* (1982) to the interpolation algorithm used in the present study, the minimum grid size for the C3 map data was 188 m and for the A2 map data, 115 m. These amounts, although calculated through the above simplifications, should justify the statement already made about over-sampling the terrain relief as depicted on the maps. Richardus, in his Table 1, shows that a 30-m contour interval is sufficient for slopes of approximately 45°, and therefore it would appear that short wavelength (high frequency) components of the mapped terrain are adequately sampled. Since the interpolation used was of a bilinear nature, the frequency response of the interpolator reduces the data's high frequency component and, therefore, minimizes aliasing effects, which would introduce artifacts into the data.

The variation of the results found between the 25 m and 100 m grids was attributed to interpolation behaviour and possible local undersampling of aliasing. The assumption of a mean slope value in the calculation of the total map error was the most probable contributor to this deviation in error. Optimum sampling intervals for interpolation of photogrammetrically DEMs are specific to terrain ruggedness (Balce, 1987) and are generally defined by using densely sampled profiles across various terrain types (Fritsch, 1988; Tempfli, 1986; Frederiksen *et al.,* 1986). The feasibility of making such profile studies is limited for users whose only source of DEM data is contoured topographic maps. In making comparisons between DEMs formed from cartographic or map sources and photogrammetrically captured ones, Faintich (1984) refers to the need for data between contours when terrain models described by these contours are to be used for interpolation. Otherwise, Faintich continues, contoured data should be used only for contour regeneration.

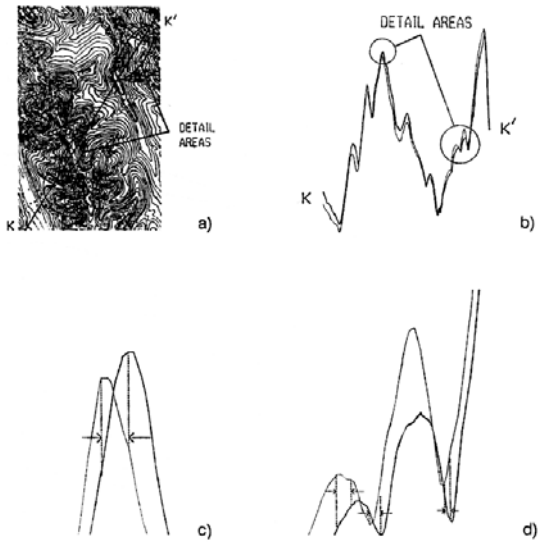

Figure 2
Profiles taken across the two map compilations illustrate that planimetric shifts at identical terrain breakpoints contribute large fluctuations in the slope-aspect differences.

(a) the area of 82G14 (old compilation) transected by K,K';
(b) the profile K,K' showing differences in old and new compilations, elevation magnification × 10; and
(c, d) details from (b), slope-aspect is potentially 180° different between the compilations.

REMOTE SENSING CONSIDERATIONS

This paper has focussed on the incident angle variations caused by uncertainty in topographic relief data. Both the incidence and emergent (existance) angles are used in surface reflectance models, such as the Lambertian and Minnaert models (Woodham *et al.,* 1985; Woodham and Lee, 1985). The Lambertian model, for instance, contains a term for the cosine of the incidence angle to describe the topographic component of energy in a returned picture element originating from direct collimated illumination. The same model describes the diffuse illumination component by the cosine of the emergent angle (ibid). Both of these angles are related to the normal vector at each point of terrain relief and will consequently be affected by the uncertainty in the vector's position.

Plunkett and Schanzer (1989) use the cosines of incidence and emergent angles to describe visibility of terrain information implicit in DEM data. They show that a variation in the incidence angle derived from different numerical models applied to the same DEM data created significant positional deflections along breaklines, such as valleys and ridges. In these areas, where a maximum slope-aspect error would be expected, a ridge location described on a synthetic image by tracing the locus of points where the emergent angle takes a value of zero degrees (cosine equal to 1) would be displaced by many pixels using the results shown in Table 2. For example, in

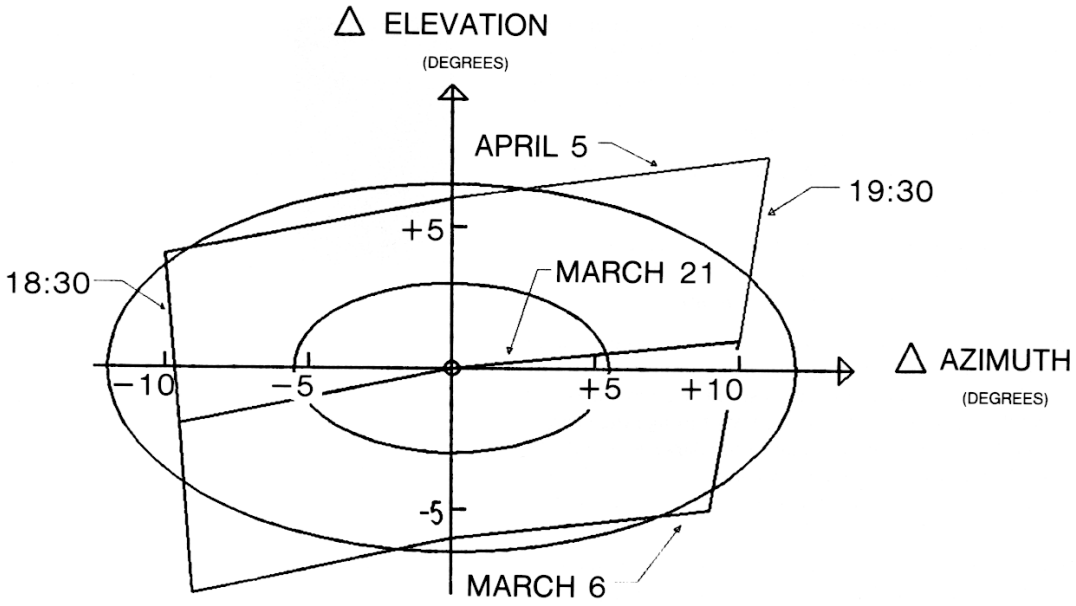

Figure 3
The origin specifies the difference in sun angles (elevation and azimuth) at UT 19:00 for March 21 at geographic co-ordinates for the test area. These times and dates correspond to the overpass time of LANDSAT-5 TM. The central disk is the solar diameter of ½° with the first ellipse's principal axis calculated from the RMS error for sun angle variations using a 100 m DEM grid and the outer ellipse for the 25 m grid. The near vertical sides of the overlaying polygons are constant time, on the dates shown by the near horizontal sides of the polygons. Uncertainty in terrain slope and slope-aspect are visualized here as being within the limits of uncertainty in solar angles.

the masked areas where a selection was made on the basis of slope-aspect differences greater than 90 degrees, the mean value for the difference in the emergent angle using 100 m data was found to be 7.3 degrees with an RMS error of 3.1; for 25 m data, the values were 24 and 11 degrees, respectively. The errors in position of ridges from uncertainty in map accuracy outweighed the displacement found by Plunkett and Schanzer .

A simple calculation on a model ridge, which has a cylindrical cross-section, shows that, for the ridge position not to change by more than one pixel on average, the radius of curvature of the cylinder must be less than 31 m for the 25 m case. These curvatures are too large for the terrain used in this study. However, with a lower mean value of the differences in emergent angle for 100 m data, this radius becomes 410 m. An estimate of 300 m for the radius of curvature of the ridge in Figure 2c helps to confirm that the reduction in errors for a 100 m grid are a result of the suitability of this grid size for the terrain relief in the test area. At the 90 per cent confidence level, however, six 100 m pixels would be required.

The use of a graphical method to describe the variation in solar angles derived from the uncertainty in slope and slope-aspect enables an interesting comparison to be made with the daily and seasonal variation of the sun position. In Figure 3, the solar diameter is contrasted with ellipses where the principal axes are the RMS errors in solar azimuth and elevations obtained from Table 2. The polygons superimposed on the ellipses are traces of the sun's position through an hour's time interval and through a monthly variation (March 6 to April5). At the origin of these variations is the sun ephemeris on March 21 at LANDSAT-5, Thematic Mapper overpass times. The displacement of the solar position (ellipses), contained in the interval of approximately one hour and one calendar month, suggests that when DEM errors are of the magnitude of this C3 map, precise ephemeris data need not be obtained for such calculations as shadow masks (Teillet *et al.,* 1986).

CONCLUSIONS

The variations in elevations, slope, and slope-aspect have been calculated from independently created digital elevation models (DEMs) derived from two sets of contour data digitized over identical geographic locations. The two sets of elevations are examined as representative of the difference in the map accuracies described as C3 (compiled 1957) and A2 (compiled 1975). Variations in the incidence angle were transformed to uncertainty in sun angles (elevation and azimuth) by fixing the sun in the co-ordinate system of the image but referring the surface normals used in the incidence angle calculation to the C3 data. The effects of unknowingly using the data from a map with an accuracy of magnitude 'C3' in a remote sensing application was therefore simulated. This description of the uncertainty in relief and terrain features, as well as the

variation in sun angles, has little generality for other instances of map accuracy or relief variation outside the test area being considered. Interpolation methodology for the creation of the DEM and its derivatives was, likewise, specific to this application and could not be used in a general statement concerning the use of maps with uncertain accuracy.

A synopsis of the differences found in the two map compilations is given in Table 2, with the final rows of this table illustrated in part in Figure 3. The topographic component in the returned energy from a remotely sensed pixel in the test area should not be modeled by synthetic means using the C3 map's elevation as input unless the application did not also require precise knowledge of the sun's ephemeris.

From CCSM (1984), in Section 4.5.5, "Utilizing a Map With No History," the following suggestion was made and applies equally in the present context:

In cases where it is impossible to make an estimate with any degree of certainty, the accuracy of the digital data (topographic) should be classified as unknown.

Therefore, the conclusion reflects the need for users of topographic relief data (specifically from NTS maps at 1:50000) to determine, or otherwise acquire, a published map's accuracy before integrating it with remotely sensed data. Map uncertainty propagates through numerical processes used in pixel classification and radiometric/atmospheric correction. The planimetric errors in geocoding using map co-ordinates and elevations interpolated from map contours has not been addressed in this work and is a subject urgently requiring further research.

ACKNOWLEDGEMENTS

This work would not have been possible without the assistance of A. Gagne and J. MacDonald of the Topographic Surveys Division of the Canada Centre for Mapping. Through their efforts, the recompilation of a new elevation basis was achieved for the test area, and considerable time was spent in helpful discussions and explanations of map accuracy standards. The author wishes to acknowledge the helpful discussions with his colleagues, in particular, Dr. B. Guindon and Dr. J. Gibbson, and also the patient typing of the numerous versions to this manuscript by A. Kalil.

Appendix I

Two identically located square facets (in planimetry), which represent a grid cell from independent DEM interpolation (Figure AI.1), can be described by their normal vectors A and A' using direction cosines (ℓ_1, ℓ_2, ℓ_3) in an earth-centred Cartesian co-ordinate system (X_1, X_2, X_3), where X_3 is the local normal and X_2 is a reference direction usually considered as a northward-pointing vector. The capital letters in the text and figures refer to vector quantities. The two facets are independent and can be assigned their own fixed co-ordinate geometries using A and A' × A (vector cross-product) for two orthogonal axis of an unprimed system, and A' and A' × A for the orthogonal axis of a primed system. Clearly, from Figure AI.2, since A' × A is normal to the plane containing the vectors A' and A, A' can be rotated by an angle θ about the vertical axis (N) to bring the two vectors into coincidence.

The incidence angles i' and i in Figure AI.2 refer to a vector S, which is defined in the co-ordinate system X_1, X_2, and X_3. Rotation by θ about N also changes S to S' with new direction cosines in X_1, X_2, and X_3. The complete geometry with reference to geographic co-ordinates (X_1, X_2, X_3) is shown in Figure AI.3.

Direction cosines taken with respect to the Cartesian system (X_1, X_2, X_3) are the unit vectors for S and N and are (a_1, a_2, a_3) and (e_1, e_2, e_3), respectively. The general rotation transformation (T_θ) about N is given by Markley (1978):

$$T_\theta = (\mathrm{Cos}\theta)\mathbf{I} + (1-\mathrm{Cos}\theta)e\hat{e} - (\mathrm{Sin}\theta)E$$

where I si the unit matrix:

$$\mathbf{I} = \begin{vmatrix} 1 & 0 & 0 \\ 0 & 1 & 0 \\ 0 & 0 & 1 \end{vmatrix}$$

$e\hat{e}$ an outer product of the vector components of N:

$$e\hat{e} = \begin{vmatrix} e_1e_1 & e_1e_2 & e_1e_3 \\ e_2e_1 & e_2e_2 & e_2e_3 \\ e_3e_1 & e_3e_2 & e_3e_3 \end{vmatrix}$$

and E is the Matrix:

$$E = \begin{vmatrix} 0 & e_3 & e_2 \\ e_3 & 0 & e_1 \\ e_2 & e_1 & 0 \end{vmatrix}$$

The geographic co-ordinates of S' in a rotated co-ordinate system fixed to N is the matrix product $|T_\theta|\ |a_1,a_2a_3|^T$. Conversion of direction cosines for S' in the (X_1,X_2,X_3) system to azimuth and elevation is done by normal vector algebra in a way that is analogous to the calculation of A and A' using slope and slope aspect data derived from the DEMs.

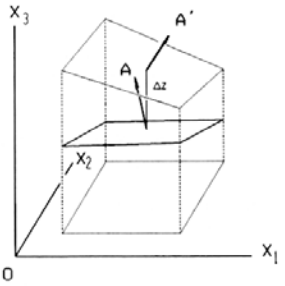

Figure AI.1
Plane facets with unit normals A' and A share identical area in (X_1,X_2) in a geographic co-ordinate system (X_1,A_2,X_3). Δz is the elevation discrepancy.

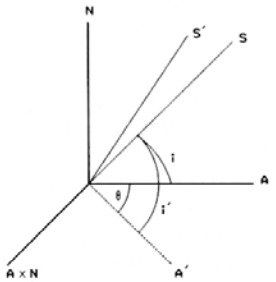

Figure AI.2
S = unit vector for the sun in a unprimed system
S' = for the primed system
i = incidence angle between sun vector S and facet normal A
i' = incidence angle between the sun vector S and the normal A'

$$\mathrm{Cos}\ (\theta) = \frac{A'oA}{|A'|\ |A|}$$ where "o" is the vector dot product

$$N = \frac{A'xA}{|A'|\ |A|\mathrm{sin}\theta}$$ where "x" is the vector cross product

and | | indicates vector magnitude.

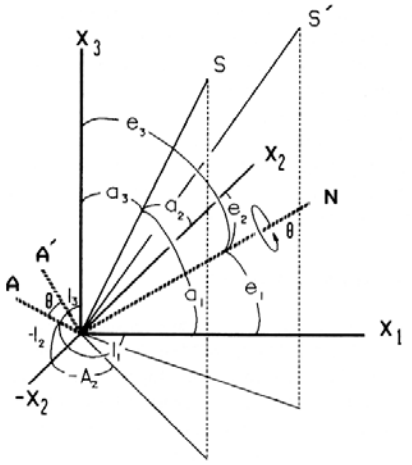

Figure A1.3

$S = (a_1, a_2, a_3)$

where $|S| = \sqrt{(a_1^2 + a_2^2 + a_3^2)} = 1$

$N = (e_1, 2_2, e_3)$

where $|N| = \sqrt{(e_1^2 + e_2^2 + e_3^2)} = 1$

The sun's angles are defined as A_z (azimuth), which is conventionally taken from a north-pointing vector (X_2), and elevation, which is calculated from a_3 since X_3 is considered as a local vertical.

S' represents the new sun position after rotation of co-ordinate system (N,A,NxA) fixed to S. From S' in (X_1,X_2,X_3) the new azimuth and elevation angles are measured.

REFERENCES

Balce, A.E. (1987) - *Determination of Optimum Sampling Interval in Grid Digital Elevation Models (DEM) Data Acquisition,* Photogrammetric Engineering and Remote Sensing, 53(3), pp. 323-330.

BCMF (1987) - Private Communication, *Forest Cover Map Series,* Inventory Branch, Ministry of Forests and Lands, Province of British Columbia.

CCM (1989) - *Map Evaluation Report,* Topographical Survey Division, Canada Centre for Mapping, June 6, 1989, pp. 2-3.

CCSM (1984) - *National Standards for the Exchange of Digital Topographic Data,* Canadian Council on Survey and Mapping, Second Draft Report, July 1984, pp. 41-54.

Clarke, A.L., Omen, A., and Loon, J.C. (1982) - *The Application of Contour Data for Generating High Fidelity Digital Elevation Models,* Auto Carto, pp. 213-222.

Faintich, M.B. (1984) - *State-of-the-Art and Future Needs for Development of Digital Terrain Models,* xv International Archives of Photogrammetry and Remote Sensing, Commission III, XXV (A3a), Rio de Janeiro, Brazil, pp. 180-196.

Frederiksen, P ., Jacobi, 0., and Kabik, K. (1984) - *Modelling and Classifying Terrain,* Proceedings, XV International Archives of Photogrammetry and Remote Sensing, Commission III, XXV (A3a), Rio de Janeiro, Brazil, pp. 258-267.

Frederiksen,P., Jacobi, 0., and Kabik, K. (1986) - *Optimum Sample Spacing in Digital Elevation Models,* Proceedings of the Symposium from Analytical to Digital, International Society for Photogrammetry and Remote Sensing, Commission III, XXVl (3/C), Rovaniemi, Finland, pp. 252-259.

Fritsch, D. (1988) - *Some Experience with the Determination of the Optimum Sampling Density,* Proceedings, XVl International Archives of Photogrammetry and Remote Sensing, Commission III, XXVll (Bll), Kyoto, Japan, pp. 463-474.

Fung, K., and Lasserre, M. (1987) - *On the Establishment of Positional Control for Remote Sensing Sensors,* Proceedings, 11th Canadian Symposium on Remote Sensing, Waterloo, Ontario, June 22-25,1987, pp. 661-670.

Gagne, A. (1986) - Private Communications, Topographic Survey Division, Surveys and Mapping Branch, Energy Mines and Resources, Ottawa, Ontario.

Goodenough, D.G., Fung, K., and Geekie, M. (1988) - *On the Integration of a Geographical Information System with LANDSAT-5,* Vision Interface, 1988, Edmonton, Alberta, June 8, 1988.

MacDonald, I. (1986) - Private Communications, Topographic Survey Division, Surveys and Mapping Branch, Energy Mines and Resources, Ottawa, Ontario.

Markley, F.L. (1978) - *Three-Axis Altitude Determination Methods, in* Spacecraft Altitude Determination and Control, 1.R. Wertz (ed.), D. Reidel Publishing Company, Boston, Massachussetts, pp. 410-428.

NATO (1983) -*STANAG* 2214, *Standardization Agreement,* Evaluation of Land Maps, Edition 4, December 13, 1983.

Ostman, A. (1987) - *Accuracy Estimation of Digital Elevation Data Banks,* Photogrammetric Engineering and Remote Sensing, 53(4), pp. 425-430.

Peucker, T.K., Fowler, R.K., Little, 1.1., and Mark, D.M. (1976) - *Digital Representation of Three-Dimensional Surfaces by Triangulated Irregular Networks (TIN),* Technical Report 10-R, Office of Naval Research, Geographic Programs, Arlington, Virginia.

Plunkett, G., and Schanzer, D. (1989) - *The Use of Synthetic Solar Illumination for Visualizing Digital Elevation Models,* ASPRS/ACSM, Fall Convention, Cleveland, Ohio, September 17-21, 1989.

Richardus, P. (1973) - *The Precision of Contour Lines and Contour Intervals of Large-and Medium-Scale Maps,* Photogrammetria, pp.81-107.

Slama, C.C., ed. (1980) - Manual of Photogrammetry, Fourth Edition, American Society of Photogrammetry, 105N Virginia Ave., Falls Church, Virginia, 22046.

Teillet, P .M., Lasserre, M., and Vigneault, C.G. (1986) - *An Evaluation of Sun Angle Computation Algorithms,* Proceedings, 10th Canadian Symposium on Remote Sensing, Edmonton, Alberta, pp. 91-100.

Tempfli, K. (1986) - *Progressive Sampling: Fidelity and Accuracy*, Proceedings of the Symposium 'From Analytical to Digital', International Society for Photogrammetry and Remote Sensing, Commission III, XXVI (3/2), Rovaniemi, Finland, pp. 653-664.

Woodham, R.J., Calanzariti, E., and Mackworth, A.K. (1985) - *Analysis by Synthesis in Computational Vision with Application to Remote Sensing*, Computational Intelligence, 2(1), pp. 71-79.

Woodham, R.J., and Lee, T.K. (1985) - *Photometric Method for Radiometric Correction of Multispectral Scanner Data*, Canadian Journal of Remote Sensing, 2(11), pp. 132-161.